THE ASTROPHYSICAL JOURNAL, 395:L13–L16, 1992 August 10

ULTRAVIOLET IMAGING TELESCOPE OBSERVATIONS OF THE CRAB NEBULA

GREGORY S. HENNESSY,[1] ROBERT W. O'CONNELL,[1] KWANG P. CHENG,[2] RALPH C. BOHLIN,[3]
NICHOLAS R. COLLINS,[4] THEODORE R. GULL,[2] PAUL HINTZEN,[2,5] JOAN E. ISENSEE,[4]
WAYNE B. LANDSMAN,[4] MORTON S. ROBERTS,[6] ANDREW M. SMITH,[2]
ERIC P. SMITH,[2] AND THEODORE P. STECHER[2]
Received 1992 March 31; accepted 1992 May 27

ABSTRACT

We obtained ultraviolet images of the Crab Nebula with the Ultraviolet Imaging Telescope (UIT) during the *Astro-1* Space Shuttle mission in 1990 December. The UV continuum morphology of the Crab is generally similar to that in the optical region, but the wispy structures are less conspicuous in the UV and X-ray. UV line emission from the thermal filaments is not strong. UV spectral index maps with a resolution of 10″ show a significant gradient across the nebula, with the outer parts being redder, as expected from synchrotron losses. The location of the bluest synchrotron continuum does not coincide with the pulsar.

Subject headings: supernova remnants — ISM: individual objects (Crab Nebula)

1. INTRODUCTION

The Crab Nebula was the first confirmed cosmic source of synchrotron radiation (Shklovsky 1953; Dombrovsky 1954; Oort & Walraven 1956). Its broad-band continuum has been detected throughout the electromagnetic spectrum and has been the subject of many studies (e.g., Baldwin 1971; Craig et al. 1985). Scargle (1969) examined structural variability in the optical continuum induced by the pulsar. He also found that the spectral index α (where $F_\nu \sim \nu^{-\alpha}$) was smaller (i.e., the light was bluer) near the center of the nebula, presumably because of synchrotron losses by the relativistic electrons as they move outward. The energy distribution of the Crab (in νf_ν units) peaks in the extreme ultraviolet/soft X-ray, which makes ultraviolet observations of particular interest. Earlier UV observations of the Crab were made by Wu (1981) and by Davidson et al. (1982). Davidson et al. used *IUE* to obtain C IV λ155 nm, He II λ164 nm, and C III] λ191 nm emission line intensities and upper limits on other UV lines. Wu published *ANS* photometry for the central 2.′5 × 2.′5 in five ultraviolet bands. He found that the UV data could be fitted with a power law with $\alpha \sim 0.50$.

The large angular size of the Crab (almost 6′ diameter) and its high UV surface brightness make it an excellent subject for imaging with the Ultraviolet Imaging Telescope (UIT).

2. OBSERVATIONS AND REDUCTIONS

The nebula was observed with the UIT for one orbital night during the *Astro-1* mission in 1990 December. The UIT is a 38 cm f/9 Ritchey-Chretien telescope with a 40′ field of view which employs intensified film cameras as detectors. Details on its specifications and performance during the mission are available in Stecher et al. (1992). We obtained eight exposures of the Crab in three different filters. The reductions concentrated almost exclusively on the longest exposure in each filter. The filters used were A1 (centroid 249 nm, bandwidth 115 nm) for 470 s exposure time, B1 (152 nm, 35 nm) for 471 s, and B5 (162 nm, 23 nm) for 390 s. These nominal centroids were calculated for a flat incident spectrum; the effective centroids change with the source spectrum, as discussed below. The film was digitized with a 20 μm aperture to 1.″14 pixels, flat fielded, and flux calibrated as described in Stecher et al. (1992). We will quote magnitudes in the monochromatic system, defined as $m_\lambda = -2.5 \log F_\lambda - 21.1$, where F_λ is in units of ergs s^{-1} cm^{-2} Å^{-1}.

The sky background in the UV is in general lower than in the optical (O'Connell 1987; Henry 1991). The background near the Crab was nonuniform, unlike most high Galactic latitude UIT fields. The A1 and B1 images show increased sky brightness at the northeast and southwest edges of the 40′ diameter frame. For better sky correction, we made two-dimensional polynomial models of the sky. The mean value of the background in boxes 45″ on a side was obtained from approximately 150 places on each frame, covering about 7% of the field of view. The estimated sky brightness in the center of the three frames, in mag arcsec^{-2}, is 24.2, 23.2, and 21.9 for the A1, B1, and B5 frames, respectively. (These values have not been corrected for residual photographic fog; the B5 frame exposure continued into the daylight side of the orbit.) The A1 and B1 frames have a "valley" of darker sky (by about 1.5 mag arcsec^{-2}) running at an angle of 130° east from north, roughly parallel to the Galactic plane. Due to the low Galactic latitude $|b| \sim 6°$, the most likely cause of the unusual background is scattering from a nonuniform dust distribution near the line of sight. Paresce et al. (1979) have reported brighter background UV radiation near the Galactic plane, $|b| \leq 10°$, with some of the sky brightness being scattering of OB starlight from dust clouds.

The Crab observations were made early in the mission, before fine tuning of the guiding system was achieved. The resulting point spread functions (PSFs) are relatively large. On the A1 exposure the stellar images are elliptical, with a FWHM of 3.″9 × 4.″3. The PSFs of the B1 and B5 frames are more circular, with FWHM of 5.″1 and 3.″6, respectively. Comparison of the total sky-subtracted flux measured on the three frames

[1] Astronomy Department, University of Virginia, P.O. Box 3818, Charlottesville, VA, 22903.
[2] Laboratory for Astronomy and Solar Physics, Goddard Space Flight Center, Greenbelt, MD 20771.
[3] Space Telescope Science Institute, 3700 San Martin Drive, Baltimore, MD, 21218.
[4] Hughes/STX, Goddard Space Flight Center, Greenbelt, MD 20771.
[5] Department of Physics, University of Nevada, Las Vegas, NV 89154.
[6] National Radio Astronomy Observatory, Edgemont Road, Charlottesville, VA, 22903.

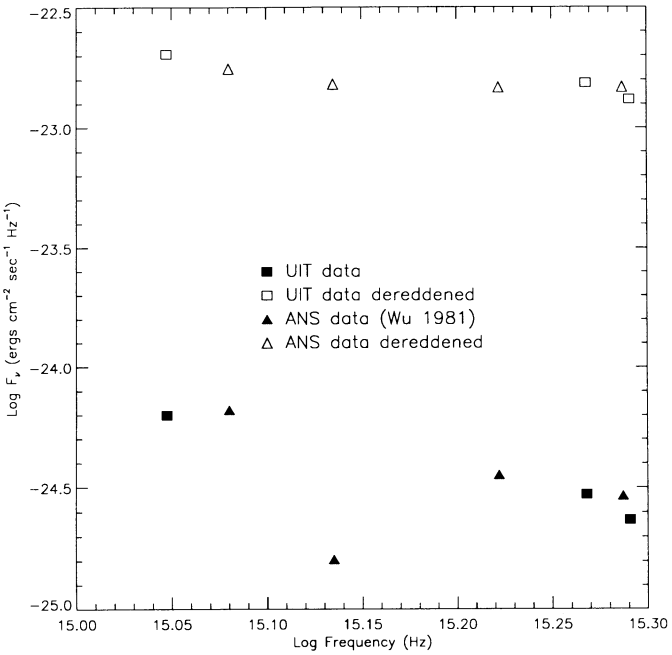

FIG. 1.—Comparison of the observed and dereddened UV fluxes of the Crab Nebula as measured by *ANS* and UIT with a 150 arcsec^2 aperture. The dereddening method is described in the text.

within a 2.5 × 2.5 square aperture centered on the pulsar to Wu's *ANS* photometry corrected to the *IUE* calibration as in Bohlin et al. (1990) is shown in Figure 1. The agreement is excellent, especially considering the length of time since the UIT laboratory calibration (1985). The mean far-UV (FUV) dereddened flux from the B1 and B5 frames matches Wu's at 155 nm to within 4%.

3. RESULTS

Our UV frames are compared to optical and X-ray images in Figure 2 (Plate L6). The overall morphology of the UV continuum is similar to that in the optical. However, the light distribution is smoother in the UV than in the optical. The fine scale structure near the pulsar, such as the "wisps" and the "anvil" (cf. Scargle 1969) is less conspicuous. Optical continuum images kindly provided by R. Fesen and W. Blair were convolved to match the resolution of the NUV image and show that the surface brightness of the bright wisps NW of the pulsar is roughly 0.4 mag arcsec^{-2} brighter than the nearby background at 477 nm. The excess surface brightness in the NUV is less than 0.2 mag arcsec^{-2}. This apparent steepening of the spectral index between the diffuse background and the wisps is also visible in the X-ray image. Although the maximum X-ray surface brightness occurs NW of the pulsar, it does not coincide with the bright wisps in the optical. The UV and X-ray appearance of the wisps would be consistent with stronger synchrotron losses due to a larger magnetic field in these time-variable features (Scargle 1969).

The eastern "bay" is conspicuous in both the NUV and optical bands, but the south-eastern quadrant is noticeably less bright in the FUV and considerably fainter in the X-ray image. The nebula overall is smaller and less symmetric with respect to the pulsar's location in the X-ray than at longer wavelengths (Harnden & Seward 1984). The FWHM of fits to slices taken along the optical major axis (P.A. = 135°) for the optical, NUV, FUV, and X-ray data are 106″, 77″, 65″, and 44″, respectively, while for the optical minor axis (45°) values were 80″, 61″, 57″, and 53″.

There are no obvious emission-line filaments on the UV images, including the B5 exposure which should be most sensitive to C IV 155 nm and He II 164 nm emission. This is in contrast to the optical band, where care is necessary in the choice of filters to obtain images without filaments. We have searched for evidence of line emission using both spatial filtering algorithms and aperture photometry and are able to set only upper limits to the C IV and He II flux. We used an [O III] 500.7 nm CCD image to construct a set of filament and background apertures to measure the region where the [O III] emission is strongest. The 3 σ limit to the flux on the B5 exposure which could be attributed to C IV and He II was 2.1×10^{-13} ergs s^{-1} cm^{-2} in a 204 arcsec^2 aperture (the aperture size of *IUE*), which is 23% larger than the strength of C IV and He II measured in this position by Davidson et al. (1982) in long *IUE* exposures. The Hopkins Ultraviolet Telescope (HUT) (Blair et al. 1992), obtained line fluxes during the *Astro-1* mission which were over twice the *IUE* values, but these refer to a larger aperture (1972 arcsec^2 vs. 205 arcsec^2 for *IUE*) and are not directly comparable to the filament measures quoted above.

Fesen & Blair (1990) found numerous small dark spots across the face of the nebula on optical continuum images, coincident with various emission line filaments. They interpreted these as small dust clouds within the nebula. Hester et al. (1990) also reported similar features. Most were smaller than 2″, but four were larger. We inspected the UIT frames for absorption features at the locations listed by Fesen & Blair and by Hester et al. but found none. (Four dark spots visible in the northern portion of the A1 frame in Fig. 2, adjacent to regions of higher intensity a few pixels away, appear to be artifacts not removed by flat-fielding.) Comparing our images to the Fesen and Blair 477 nm image smoothed to the UIT FWHM, we find that we would not have detected dust clouds with comparable UV amplitudes and sizes. However, from the standard UV extinction law (e.g., Savage & Mathis 1979), one expects UV absorption amplitudes to be larger than in the optical. It is possible that the location of the clouds within the synchrotron nebula or UV scattering effects have reduced the UV contrast of these objects.

Although the UV nebular continuum is bright, the pulsar is just detectable on our A1 image as a faint point source near the radio pulsar coordinates ($\alpha = 05^h34^m31^s.9$ $\delta = 22°00'51''.5$, J2000). It is not convincingly present on the B1 frame. Because there are residual errors produced by *S*-distortion in the UIT image tubes, we confirmed our astrometry using field stars from an optical CCD image. We find m_λ(249 nm) ~ 18.7 and m_λ(152 nm) $\gtrsim$ 17.2 for the pulsar.

van den Bergh (1970) noted a faint jet extending about 1 pc from the northern edge of the Crab. The jet is visible in emission-line photographs (Chevalier & Gull 1975; Fesen & Gull 1986) and as synchrotron radiation in radio images (Velusamy & Roshi 1991). Our UV images do not show an extension of the nebula in this area; an upper limit for the surface brightness of the jet is μ_λ(249 nm) $\gtrsim$ 22.6 mag arcsec^{-2}.

The spectral energy distribution of the Crab has been measured over 13 decades in frequency; but until now there was no determination of the total UV flux, since the nebula has a larger angular size than the *ANS* or *IUE* apertures. Using an irregular polygonal aperture placed to include all the nebular flux while excluding field stars, we measured total fluxes for the

PLATE L6

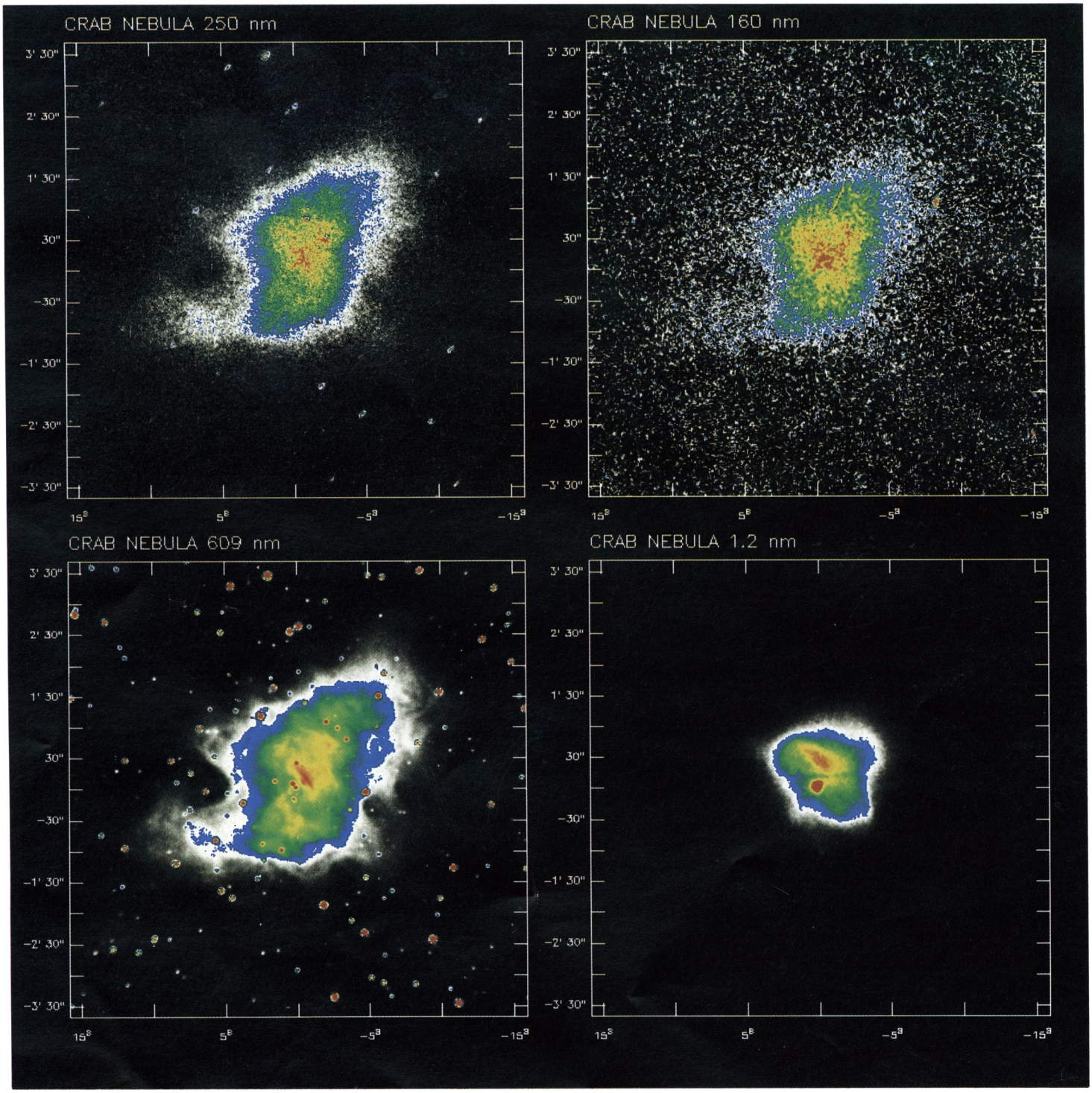

FIG. 2.—Pseudocolor images of the Crab Nebula in four wavelength bands. Each image is 512 × 512 pixels, with a pixel size of 1.″14. In the upper left is the UIT NUV image, and in the upper right is the average of the two FUV images. In the lower right is the *Einstein* HRI image (Harnden & Seward 1984), while in the lower left is an optical continuum image (emission-line free) kindly provided by Robert Fesen. The resolution of the *Einstein* image is ~8″, while the 609 nm image has a resolution of ~2″. The coordinate grids are centered on the pulsar; all four images have the same scale. The color table was selected to display both high and low values. It is set to red at the highest levels in the nebula, declining through yellow, green, blue, white, and gray, to black.

HENNESSY et al. (see 395, L14)

A1, B1, and B5 filters of 3.95, 4.17, and 4.66 $\times 10^{-13}$ ergs cm^{-2} s^{-1} Å^{-1}, respectively. The uncertainty in these values is estimated to be $\sim$15%, most of which is systematic error in the *IUE* absolute flux calibration (Bohlin et al. 1990). The ratio of the total flux to the flux in the central 150 arcsec^2 is 1.43, which is 24% lower than the value of 1.88 that Wu (1981) used to extrapolate his measurements to the whole nebula.

The exact value of the extinction towards the Crab remains somewhat unsettled (Davidson & Fesen 1985); but we choose to use a value of $E(B-V) = 0.50$, based on Wu's (1981) UV measurements of field stars and our results from Figure 5 below. Owing to the large width of the UIT filters, it is necessary to integrate the extinction law numerically through the filter response functions to obtain mean values. We adopted the shape of the Seaton (1979) law fitted to the UV extinction values measured by Wu to obtain mean extinctions for the A1, B1, and B5 filters of 3.77, 4.38, and 4.29 mag, respectively. The Wu extinction curve is only slightly different from the standard Savage & Mathis (1979) curve; using the latter would change our derived spectral indices by only $\Delta\alpha \sim -0.05$. The extinction also affects the wavelength centroids of each filter; for the observed power law and adopted extinction, these become 269, 154, and 162 nm.

The dereddened, spatially integrated fluxes are then 1.24, 2.35, and 2.42 $\times 10^{-11}$ ergs cm^{-2} s^{-1} Å^{-1}, for the A1, B1, and B5 filters. The corresponding integrated UV spectral index, corrected for reddening, is $\alpha = 0.83$. The dereddened spectral index for a centered 150 arcsec^2 aperture is $\alpha = 0.67$, somewhat steeper than Wu's measurement of $\alpha = 0.50$. Note that because $\delta\alpha \sim -4.31\delta \log [F_\lambda(\mathrm{FUV})/F_\lambda(\mathrm{NUV})]$, small uncertainties in the measured flux or extinction corrections produce appreciable changes in α (cf. also Fig. 5). The overall power law in the optical–UV is flatter than the IR–X-ray mean spectral index $\alpha \sim 1$ (Craig et al. 1985). The luminosities corresponding to these fluxes are 5.7, 3.3, and 2.2 $\times 10^{36}$ ergs s^{-1}, assuming the distance to the Crab is 1830 pc (Davidson & Fesen 1985), or equivalently 1590, 860, and 580 $L_\odot$, respectively. Davidson and Fesen estimate that the bolometric luminosity of the Crab nebula is 1.38 $\times 10^{38}$ ergs s^{-1}, implying that over 6% of its luminosity emerges in the 1200–3200 Å region.

To study changes in the continuum slope with position in the nebula, we have constructed a spectral index map. The sky-subtracted images, corrected for reddening, were converted to fluxes and then binned to 10″ (9 pixel) resolution. Based on laboratory flat-field measurements, this will increase the S/N ratio by a factor of about 5. Cells with net flux values less than 3 times the sky flux were rejected from consideration. In each cell the spectral index was determined by making a least-squares fit to the energy distribution at the effective wavelengths of the three filters.

The spectral index map is shown in Figure 3 (Plate L7), where redder areas are dark and bluer areas are light. There are conspicuous general gradients across the nebula, with the inner regions being bluer (harder radiation). The edges of the nebula are particularly red, especially the eastern bay and the southeastern portion of the nebula. These changes in spectral index are reflected in the morphological changes with wavelength in Figure 2. The general gradient is consistent with the aging of the relativistic electrons that produce the synchrotron radiation as they move out through the nebula (Woltjer 1958; Scargle 1969). Surprisingly, the hardest radiation ($\alpha \sim 0.23$) is not coincident with the pulsar but instead lies approximately 60″ to the northwest. We are unaware of other special properties associated with this area, but it does lie roughly on an extension of the line connecting the center of expansion of the nebula (Wyckoff & Murray 1977) and the current location of the pulsar. This may simply be a coincidence.

Figure 4 shows the spectral index of the dereddened images as a function of radius, for the northwest and southeast halves, bisected along a cut at 45° east from north. The sky-subtracted flux from the three frames was summed in annular rings of 10″ width, with an increment of 5″, and then the spectral index calculated for each ring. Annular averaging in this manner loses many of the interesting details from Figure 3 but shows large-scale trends in the data. This profile agrees well in its gross characteristics with the radio spectral index/radius relation found by Velusamy, Roshi, & Venugopal (1992). With the exception of the smallest annuli, the southeastern half of the nebula is systematically redder than the northwestern half and shows a greater change in the spectral index with radius. The UV/X-ray spectral indices (not shown) are similar to the NUV/FUV spectral indices in Figure 4. Both halves show the trend of a general increase of spectral index with radius. The outer limit of the plot was chosen such that the S/N of the mean annular flux was over 20 in all three UV filters.

Scargle's (1969) photometry showed that the spectral index in the optical is flattest (bluest) near the pulsar, and becomes steeper (redder) with distance, but his aperture grid did not extend out as far as the UIT spectral index minimum. In Figure 5 we show a comparison of Scargle's data and ours for his position no. 1. Scargle's data was dereddened with the curve of Savage & Mathis (1979). The data points should join smoothly, with a constant slope, assuming the incident radiation from the Crab is a power law. Figure 5 clearly illustrates the importance of the reddening correction in matching the

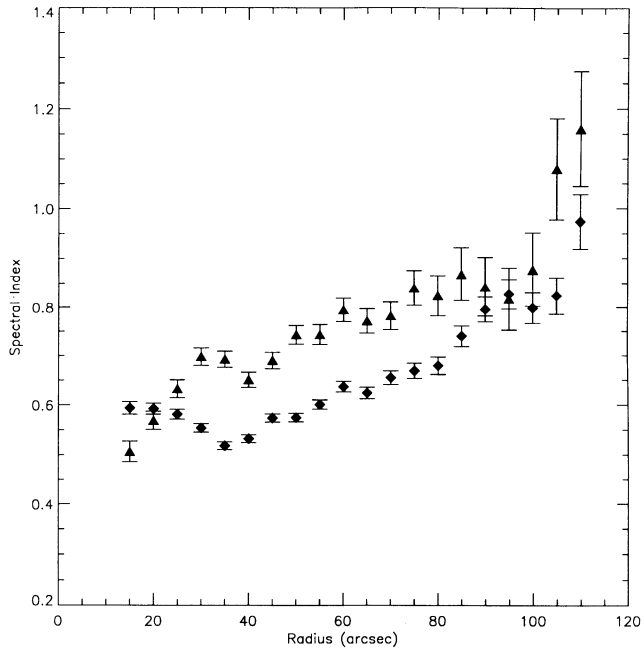

FIG. 4.—UV spectral index, corrected for reddening, in circular annuli of 10″ width centered on the pulsar as a function of radius. The triangles are for the SE semi-major axis of the nebula, while the diamonds are for the NE semi-major axis. The general steepening of the spectral index with distance is presumably from synchrotron losses. The error bars are the 1 σ errors to the fit in each annulus.

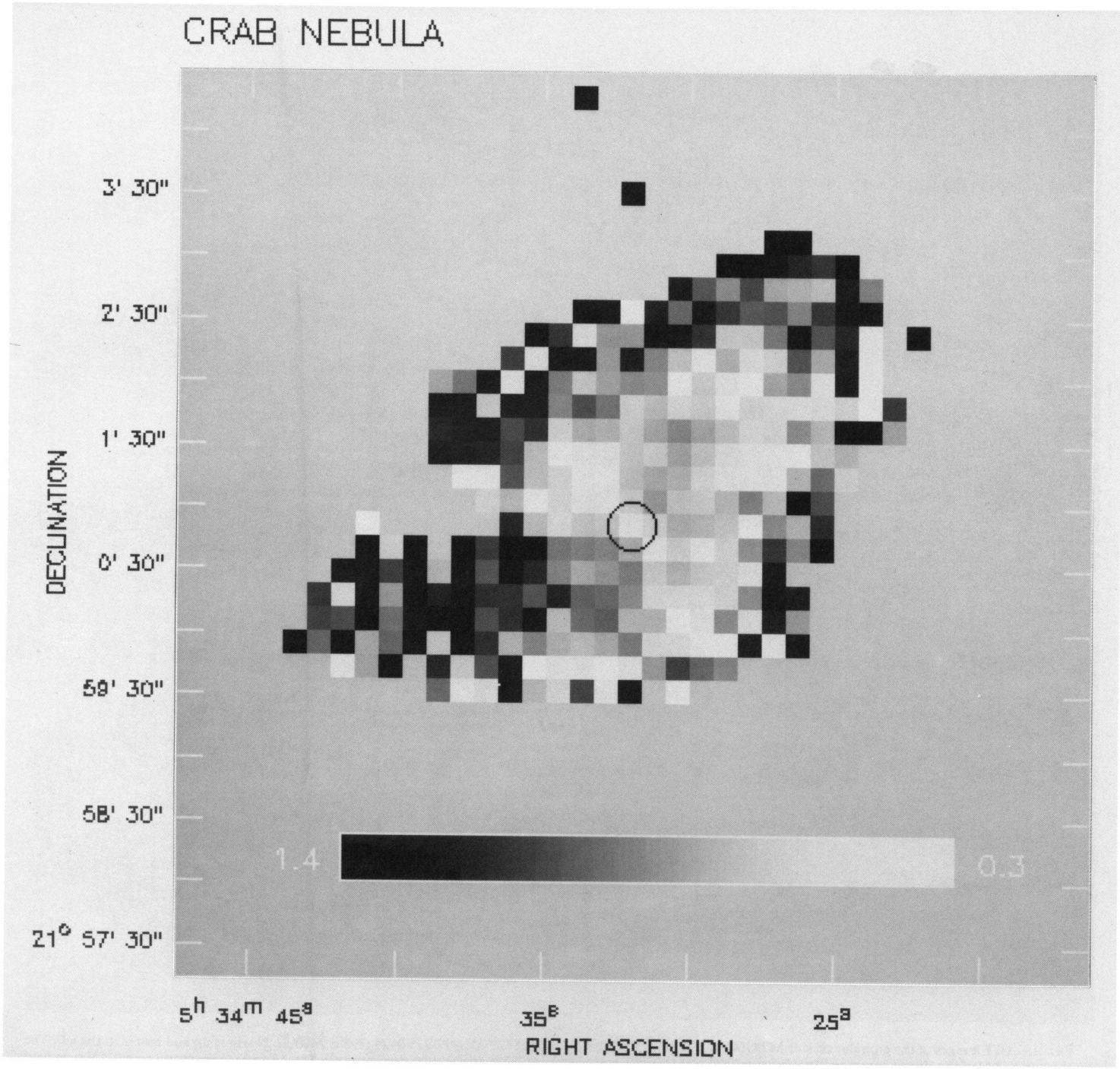

FIG. 3.—Gray-scale representation of the ultraviolet spectral index of the Crab Nebula, binned over cells of 10″. Darker areas correspond to larger spectral indices (redder light) and lighter areas to smaller indices. The inset shows the correspondence between spectral index and tone. Sky noise outside the nebula has been suppressed by setting all pixels with fluxes smaller than 3 times the sky flux to a mid-gray tone. The circle marks the position of the pulsar.

HENNESSY et al. (see 395, L15)

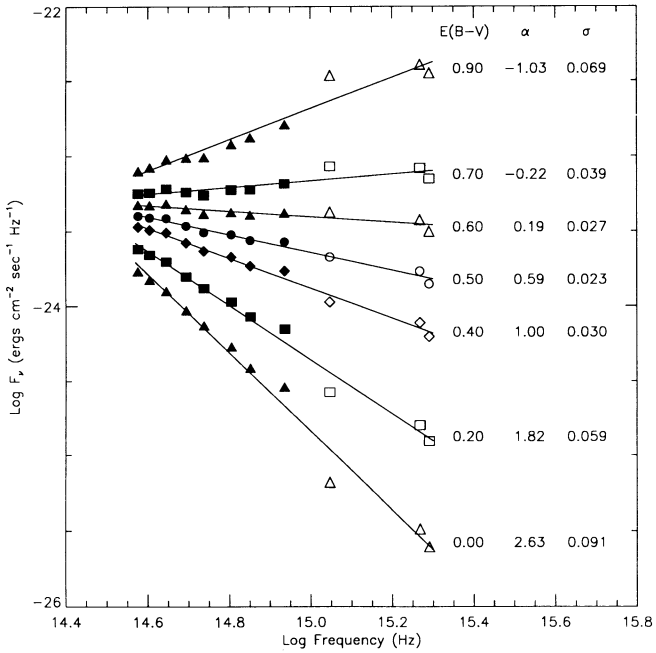

FIG. 5.—Comparison of the dereddened flux in the optical and the UV at Scargle's (1969) position no. 1. The open symbols represent UIT data while the filled symbols represent Scargle's optical data. The three columns on the right list the amount of extinction assumed, the fitted spectral index, and the standard deviation of the fit. The best fit is for an assumed $E(B-V) = 0.50$.

optical and UV data sets. The best match is for $E(B-V) \sim 0.4$–0.6, in agreement with Wu's (1981) value of 0.5. Adopting this value, we find the UIT spectral indices are systematically redder than Scargle's other measures over the region in common, but the trends are similar. The discrepancies do not appear significant, given the uncertainty in the reddening law.

4. CONCLUSIONS

The UV continuum morphology of the Crab Nebula is generally similar to that in the optical region but is affected by wavelength-dependent trends which become yet more pronounced in the X-ray. The continuum wisps are less conspicuous at higher energies than in the optical. We do not detect bright C IV emission or dust clouds of size $\gtrsim 5''$. Mean fluxes obtained in the central 150″ are in excellent agreement with *ANS* values. The nebula emits over 6% of its bolometric luminosity in the 1200–3200 Å region. Spectral index maps of the nebula show significant UV color gradients, with the edges of the nebula having larger spectral indices than the central regions, as expected from synchrotron losses. There is a significant color asymmetry between the NW and SE semi-major axes of the nebula. The hardest radiation is found not in the area adjacent to the pulsar but rather about 60″ NW. This may be the site of an interaction between a relativistic wind from the pulsar and the shell of the nebula, or a region of strong in situ acceleration of the relativistic electrons.

We would like to thank Robert Fesen and Bill Blair for providing digital data in advance of publication. We gratefully acknowledge the innumerable contributions made by the hundreds of people involved in the *Astro-1* mission. We also thank the referee for comments which improved this *Letter*. This research was supported in part by NASA grants NAG5-700 and NAGW-2596 to the University of Virginia.

REFERENCES

Baldwin, J. E. 1971, in IAU Symp. 46, The Crab Nebula, ed. R. D. Davies & F. G. Smith (Dordrecht: Reidel), 26
Blair, W. P., et al. 1992, ApJ, in press
Bohlin, R. C., Harris, A. W., Holm, A. V., & Gry, C. 1990, ApJS, 73, 413
Chevalier, R. A., & Gull, T. R. 1975, ApJ, 200, 399
Craig, I. J. D., McClements, K. G., Thompson, A. M., & Brown, J. C. 1985, A&A, 149, 171
Davidson, K., & Fesen, R. A. 1985, ARA&A, 23, 119
Davidson, K., et al. 1982, ApJ, 253, 696
Dombrovsky, V. A. 1954, Dokl. Akad. Nauk SSR, 94, 1021
Fesen, R. A., & Blair, W. P. 1990, ApJ, 351, L45
Fesen, R. A., & Gull, T. R. 1986, ApJ, 306, 259
Harnden, F. R., & Seward, F. D. 1984, ApJ, 283, 279
Henry, C. H. 1991, ARA&A, 29, 89
Hester, J. J., Graham, J. R., Beichman, C. A., & Gautier III, T. N. 1990, ApJ, 357, 539
O'Connell, R. W. 1987, AJ, 94, 876
Oort, J. H., & Walraven, T. 1956, Bull. Astron. Inst. Netherlands, 12, 285
Paresce, F., Margon, B., Bowyer, S., & Lampton, M. 1979, ApJ, 230, 304
Savage, B. D., & Mathis, J. S. 1979, ARA&A, 17, 73
Scargle, J. D. 1969, ApJ, 156, 401
Seaton, M. J. 1979, MNRAS, 187, 73P
Shklovsky, I. S. 1953, Dokl, Akad. Nauk SSSR, 90, 983
Stecher, T. P., et al. 1992, ApJ, 395, L1
van den Bergh, S. 1970, ApJ, 160, L27
Velusamy, T., & Roshi, D. 1991, Current Sci., 60, 120
Velusamy, T., Roshi, D., & Venugopal, V. R. 1992, MNRAS, 255, 210
Woltjer, L. 1958, Bull. Astron. Inst. Netherlands, 14, 39
Wu, C.-C. 1981, ApJ, 245, 581
Wyckoff, S., & Murray, C. A. 1977, MNRAS, 180, 717